Motion Control of Robotic Fish Under Dynamic Environmental Conditions Using Adaptive Control Approach

Saurab Verma, *Student Member, IEEE*, Dong Shen, *Member, IEEE*, and Jian-Xin Xu, *Fellow, IEEE*

***Abstract*—In this paper, we propose a novel robust adaptive control technique to steer the direction of attack of the robotic fish swimming under influence from varying environmental conditions. Due to complex nature of robot motion hydrodynamics, it is difficult to predict the true dynamics of the system with good accuracy. Hence, a discrete-time adaptive control technique is proposed, which can effectively track a reference even if the robot system's model parameters might vary over time due to physical variations in the system. Rigorous theoretical convergence analysis on the closed-loop system confirms that the reference tracking error will asymptotically be bounded within a prescribed limit. Furthermore, the adaptive control approach is experimentally verified to produce desirable performance under significant variations in payload and drag force on the robotic fish. The latest results, thus, signify that the proposed control algorithm can efficiently control the robotic fish motion in complex underwater environments.**

***Index Terms*—Adaptive control, discrete-time system, motion control, robotic fish, unstructured environment.**

I. Introduction

ROBOTIC fish are proposed to be the next generation of autonomous underwater vehicles (AUVs) portraying desirable features such as higher agility, lower noise to the surroundings, and higher power efficiencies; features which are generally not common in the traditional rotary-propeller-based AUVs [1]–[4]. For this reason, over the past two decades, there have been several developments in the field of robotic fish systems including hardware [5], [6], sensors [7], [8], build materials [9], [10], and task completion [11]–[14] perspectives. Yet, not much development has been initiated on the motion control of robotic fish. The primary reason for the difficulty in motion control is that the robotic fish swimming mechanism is a highly intricate process in which the motion thrust is an external reactive force on the robot [15], [16]. Body undulations performed by the robotic fish apply an unsteady force on the surrounding waters in an opposite direction and, in turn generates the required reactive thrust to propel itself forward [17]–[21]. Such an unsteady motion thrust generation mechanism is difficult to be modeled accurately, especially due to strong influence from complex fluid dynamics [22]–[24]. Hence, this hinders the applicability of most of the control strategies for robotic fish motion control [25]–[28].

Recently, a few substantial improvements on linear speed control of robotic fish swimming in one-dimension (1-D) have been achieved. For example, simulations results shown in [29] confirm acceptably well control performance by fuzzy logic control (FLC) when applied to the linear motion speed control of a robotic fish. However, since FLC significantly rely on information from user experience with a particular prototype, the control technique cannot be generalized to all robotic fish. To provide robustness against updates in physical form of the robot prototypes, iterative learning control (ILC) was proposed in [30] to minimize the linear speed tracking error over multiple iterations. Since ILC learns the system behavior iteratively using experimental data, any physical updates implemented on the robot prototypes can be easily learned in subsequent iterations. Yet, robustness against environmental variations in real-time implementation cannot be guaranteed either by FLC or ILC because that feature requires the prediction of robot motion and thus, in turn, requires the sufficient understanding of robot dynamics. In [31] though, real-time speed control was accomplished using a robust sliding mode control technique based on a data-driven dynamical model. Analysis performed on exhaustive amounts of experimental data collected for dynamical modeling revealed highly complex nature of robotic dynamics.

Real-time direction/orientation control is equally important as linear speed control, for complete motion control of the robotic fish in a 2-D space. However, unlike in [31], it is not desirable to manually and extensively study the robot dynamics to construct a suitable direction control algorithm. Hence, in this paper, we propose a robust adaptive control technique that can update the respective dynamical model parameters to minimize the magnitude of the reference tracking error asymptotically. Therefore, the control approach intensively reduces manual efforts in correctly and completely modeling the robotic fish dynamics. Furthermore, the adaptation feature of the proposed control assures good control performance even when the system parameters or applicable environmental factors may vary.

Manuscript received December 30, 2016; revised May 12, 2017; accepted September 19, 2017. Date of publication October 25, 2017; date of current version April 12, 2018. *(Corresponding author: Saurab Verma.)*

Associate Editor: T. Maki.

S. Verma is with the Department of Electrical and Computer Engineering, National University of Singapore, Singapore 117583 (e-mail: saurabverma@u.nus.edu).

D. Shen is with the College of Information Science and Technology, Beijing University of Chemical Technology, Beijing 100029, China (e-mail: shendong@mail.buct.edu.cn).

J.-X. Xu is with the Department of Electrical Engineering, National University of Singapore, Singapore 117583 (e-mail: elexujx@nus.edu.sg).

Digital Object Identifier 10.1109/JOE.2017.2758158

While constructing the adaptive control algorithm, we adopt three systematic steps. First, a nonlinear dynamical model is constructed based on the state-of-the-art knowledge available on robotic fish dynamics. Second, using Taylor series expansion, the nonlinear model is converted to linear-in-parameter (LIP) form for ease in implementation. Third, a discrete-time adaptive control technique is proposed, on the basis of LIP dynamical model with control input saturation. Note that control input saturation occurs in a robotic fish body due to mechanical limitations of the actuators and is handled carefully in the adaptation law to guarantee tracking error convergence. Extensive convergence analysis, shown later, theoretically confirms that the tracking error asymptotically converges to within a desirable limit.

In a real-world application though, the robotic fish is expected to swim under dynamic environmental conditions. Hence, even under such dynamic scenarios, it is desirable that the proposed control algorithm produces good tracking performance. Thus, the robustness of proposed adaptive control is experimentally verified and comparisons are made among the obtained results. Specifically, two essential environmental factors are varied in the experimental trials.

First, the control algorithm is tested when an additional 25% of mass is loaded on the robotic fish. The mass of payload is expected to vary intensively during different field operations based on individual operation's requirements [32], [33]. Hence, this test signifies that the control algorithm can handle robotic fish motion even upon considerable addition of payload to the robot.

Second, the control is tested with increased drag force on the robotic fish. Increased drag force is equivalent to the force experienced while swimming an upstream [24], [34], [35], commonly experienced by AUVs operating in the field [17], [30]. Thus, the test results demonstrate the control performance while the robot is swimming against an elevated resistive force. In conclusion, results from these experimental trials conducted illustrate the effectiveness and robustness of the proposed adaptive control technique.

This paper is organized as follows. Section II establishes a dynamical model, constructs a robust adaptive control algorithm and theoretically analyzes the closed-loop reference tracking error convergence. Next, in Section III, the robotic fish platform is discussed, adaptation parameters are tuned, and robustness of adaptive control against variation in payload and drag forces on the robot. Finally, a brief conclusion is presented in Section IV.

II. Dynamical Model and Motion Control

In this section, the dynamical model and adaptive control techniques are devised. First, a dynamical model is constructed in LIP form using Taylor series expansion, starting with a nonlinear model. The LIP form construction assists significantly in adaptive control formulation. The complex hydrodynamical interactions in the robotic fish motion are retained as unknown model parameters, which can be easily estimated. Second, a control law is devised by inversion of the plant model, using estimated values of the model parameters. Third, an adaptation law for model parameters is presented. Furthermore, due to simplification of the originally nonlinear dynamical model, it is expected that perturbations exist in the model parameters. Hence, an adaptive law for estimation of the bound on the perturbations is also devised such that the steady-state error of the closed-loop system reduces in the order of bound on the perturbations.

A. Plant Model

Consider the angular motion of the robotic fish described by the discrete-time dynamical model

$$\omega_{k+1} = f_k - d_k + \nu_k^0 \tag{1}$$

where ω_k is the angular speed, f_k denotes the nonlinear motion dynamical function, d_k is the motion opposing damping force, and ν_k^0 is external disturbance. Generally, the damping force is represented as

$$d_k = a^0 \omega_k$$

with $a^0 > 0$ as a constant [36]. However, the only substantial information about nonlinear dynamics is that

$$f_k = f(\omega_k, u_k)$$

where $f(\cdot)$ is an unknown function of angular speed ω_k and the control input u_k. u_k is generally an *a priori* known kinematic parameter that leads to asymmetric body undulations in the robotic fish [25], [28], [37], [38].

Since, the nonlinear dynamical function $f(\cdot)$ is unknown, it should be converted to a parametric form for estimation. As a result, the dynamical model in (1) is linearized using Taylor Series expansion as follows:

$$\omega_{k+1} = \alpha_k \omega_k + \beta_k u_k + \nu_k^1 \tag{2}$$

where

$$\alpha_k = \left(\frac{\partial f}{\partial \omega}\bigg|_{\omega_k, u_k} - a^0 \right), \ \beta_k = \left(\frac{\partial f}{\partial u}\bigg|_{\omega_k, u_k} \right)$$

are model parameters to be estimated and

$$\nu_k^1 = \nu^0 + \left(\frac{\partial^2 f}{\partial \omega^2}\bigg|_{\omega_k, u_k} \omega_k^2 + \frac{\partial^3 f}{\partial \omega^3}\bigg|_{\omega_k, u_k} \omega_k^3 + \cdots \right) + \left(\frac{\partial^2 f}{\partial u^2}\bigg|_{\omega_k, u_k} u_k^2 + \frac{\partial^3 f}{\partial u^3}\bigg|_{\omega_k, u_k} u_k^3 + \cdots \right).$$

From the empirical data on input–output relation (collected using the robotic fish prototype described later in Section III-A) as shown in Fig. 1, it is observed that for constant u_k, generally the effect of ν_k^1 (shown by error bars) is minimal in relation to ω_k. Since the magnitude of ν_k^1 is relatively low, we consider it to be a parametric perturbation in the system and represent it as $\nu_k^1 = \delta_k^0 \omega_k + \delta_k^1 u_k$ such that (2) can be further simplified to

$$\omega_{k+1} = a_k \omega_k + b_k u_k \tag{3}$$

where $a_k = \alpha_k + \delta_k^0$ and $b_k = \beta_k + \delta_k^1$.

Once the parameter values a_k and b_k are adapted, the control signal can be constructed by inverting the plant model (3) under the condition that b_k does not change sign and is always

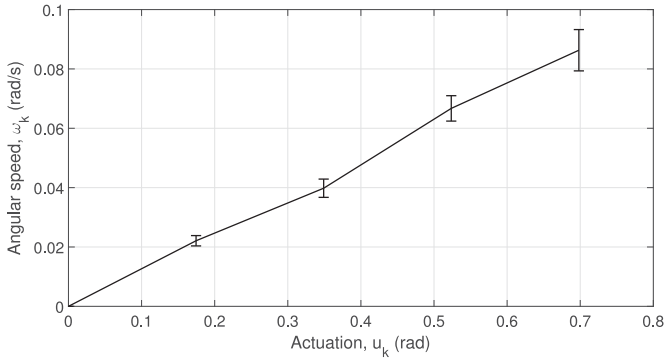

Fig. 1. Angular speed response for constant input.

nonsingular. Therefore, without loss of generality, assume that $b_k \geq b_{\min} > 0$ for some known scalar bound $b_{\min}$ [39].

Before control formulation, it should be noted that in practice, the orientation of the robotic fish ϕ_k imparts higher importance than its angular speed ω_k [3], [40], [41]. Orientation of the robotic fish is defined as the direction in which the robot body is travelling, with respect to (w.r.t.) a global inertial frame of reference. Thus, by setting a sampling time of 1 s, the following relation holds:

$$\omega_{k+1} = \frac{\phi_{k+1} - \phi_k}{1}.$$

Likewise, the dynamical model (3) is updated to

$$\phi_{k+1} = (1 + a_k)\phi_k - a_k\phi_{k-1} + b_k u_k \tag{4}$$

with ϕ_k as the state of dynamics.

B. Control Law

Since the original nonlinear model (1) is simplified to a linear model (3), the unknown model parameters a_k and b_k have a nominal parametric component $\boldsymbol{p}_*$, which can be estimated, and a high-frequency low-magnitude parametric perturbation component $\boldsymbol{\delta}_k$ such that

$$\begin{bmatrix} a_k \\ b_k \end{bmatrix} = \begin{bmatrix} \alpha \\ \beta \end{bmatrix} + \begin{bmatrix} \delta_k^0 \\ \delta_k^1 \end{bmatrix} = \boldsymbol{p}_* + \boldsymbol{\delta}_k.$$

Note that the perturbation term, $\boldsymbol{\delta}_k$ (which can be random, time varying, or state dependent in nature) is generally due to unmodeled dynamical components, external disturbance forces, etc., and, hence, must be bounded in the physical world. Hence, we have

$$\|\boldsymbol{\delta}_k\| \leq \epsilon$$

where $\|\cdot\|$ denotes the Euclidean norm and ϵ is an unknown nonnegative scalar bound.

Let $\widehat{\boldsymbol{p}}_k = [\,\widehat{\alpha}_k \;\; \widehat{\beta}_k\,]^T$ be an estimation of $\boldsymbol{p}_* = [\,\alpha_k \;\; \beta_k\,]^T$, and thus, the error in estimation is defined as

$$\widetilde{\boldsymbol{p}}_k = \begin{bmatrix} \widetilde{\alpha}_k & \widetilde{\beta}_k \end{bmatrix}^T = \boldsymbol{p}_* - \widehat{\boldsymbol{p}}_k. \tag{5}$$

Now, the control signal u_k, within $[u_{\min}, u_{\max}]$ bound due to actuator constraints, is constructed as

$$u_k = \begin{cases} u_{\min}, & \text{if } g_k < u_{\min} \\ g_k, & \text{if } u_{\min} \leq g_k \leq u_{\max} \\ u_{\max}, & \text{if } u_{\max} < g_k \end{cases} \tag{6}$$

where g_k is obtained by inverting the plant model (4) as

$$g_k = \widehat{\beta}_k^{-1}\left(\phi_{k+1}^r - (1 + \widehat{\alpha}_k)\phi_k + \widehat{\alpha}_k\phi_{k-1}\right).$$

Note that since $b_k \geq b_{\min} > 0$, it can also be stated that $\widehat{\beta}_k \geq b_{\min} > 0$, i.e., $\widehat{\beta}_k^{-1}$ exists, and hence, g_k can be computed.

Next, using the robot's dynamical model (4) and ϕ_k^r as the reference orientation, the tracking error is defined by

$$\begin{aligned} e_{k+1} &\triangleq \phi_{k+1}^r - \phi_{k+1} \\ &= \phi_{k+1}^r - (1 + a_k)\phi_k + a_k\phi_{k-1} - b_k u_k + \widehat{\beta}_k u_k - \widehat{\beta}_k u_k \\ &= -\left(1 + \alpha + \delta_k^0\right)\phi_k + \left(\alpha + \delta_k^0\right)\phi_{k-1} - \left(\widetilde{\beta} + \delta_k^1\right)u_k \\ &\quad + \phi_{k+1}^r - \widehat{\beta}_k u_k. \end{aligned}$$

For an unsaturated control signal (i.e., $u_k = g_k$), the control law (6) leads to the closed-loop error dynamics as follows:

$$\begin{aligned} e_{k+1} &= -\left(\widetilde{\alpha}_k + \delta_k^0\right)(\phi_k - \phi_{k-1}) \\ &\quad - \left(\widetilde{\beta}_k + \delta_k^1\right)\widehat{\beta}_k^{-1}\left(\phi_{k+1}^r - (1 + \widehat{\alpha}_k)\phi_k + \widehat{\alpha}_k\phi_{k-1}\right) \\ &= -\left(\widetilde{\boldsymbol{p}}_k^T + \boldsymbol{\delta}_k^T\right)\boldsymbol{\xi}_k \end{aligned} \tag{7}$$

where

$$\boldsymbol{\xi}_k = \begin{bmatrix} \phi_k - \phi_{k-1} \\ \widehat{\beta}_k^{-1}\left(\phi_{k+1}^r - (1 + \widehat{\alpha}_k)\phi_k + \widehat{\alpha}_k\phi_{k-1}\right) \end{bmatrix} = \begin{bmatrix} \omega_k \\ g_k \end{bmatrix}. \tag{8}$$

C. Adaptation Law

From closed-loop error dynamics (7), the error magnitude due to parametric perturbation $\boldsymbol{\delta}_k$ is

$$|e_k| \leq \|\boldsymbol{\delta}_{k-1}\|\|\boldsymbol{\xi}_{k-1}\| \leq \epsilon\|\boldsymbol{\xi}_{k-1}\|. \tag{9}$$

Hence, it is a logical approach to stop parameter adaptation when the tracking error magnitude $|e_k|$ decreases below the bound $\epsilon\|\boldsymbol{\xi}_{k-1}\|$. Although the value of ϵ is unknown, let

$$\epsilon = \lambda\eta \tag{10}$$

such that η is an unknown nonnegative scalar value to be estimated and $\lambda > 0$ is a tunable constant that helps control the adaptation rate for η.

Furthermore, let $\widehat{\eta}_k$ be the estimate of η; then based on the above analysis, we define a weighing coefficient $\mu_k \in [0, 1)$ as

$$\mu_k \triangleq \begin{cases} 1 - \dfrac{\lambda\widehat{\eta}_{k-1}\|\boldsymbol{\xi}_{k-1}\|}{|e_k|}, & \text{if } |e_k| \geq \lambda\widehat{\eta}_{k-1}\|\boldsymbol{\xi}_{k-1}\| \\ 0, & \text{if } |e_k| < \lambda\widehat{\eta}_{k-1}\|\boldsymbol{\xi}_{k-1}\|. \end{cases} \tag{11}$$

The weighing coefficient μ_k helps control the parameter adaptation rate in proportion to the error magnitude. Additionally, μ_k is equated to zero when the error magnitude lowers below the respective level as described in (9).

Now, $\widehat{\eta}_k$ is estimated as

$$\widehat{\eta}_k = \widehat{\eta}_{k-1} + \frac{\mu_k \gamma \lambda \|\boldsymbol{\xi}_{k-1}\| |e_k|}{\psi_k}. \tag{12}$$

Here, the denominator term is defined as

$$\psi_k \triangleq 1 + \boldsymbol{\xi}_{k-1}^T \Gamma \boldsymbol{\xi}_{k-1} + \gamma \lambda^2 \|\boldsymbol{\xi}_{k-1}\|^2 \geq 1 \tag{13}$$

where $\Gamma = \Gamma^T > 0$, being a 2×2 positive definite matrix, and $\gamma > 0$, being a positive scalar, are two tunable constants and $e_k, \zeta_k, \lambda, \mu_k$ are as defined in (7), (8), (10), and (11), respectively.

Starting with $\widehat{\eta}_0 = 0$, the adaptation algorithm in (12) ensures that $\widehat{\eta}_k$ value should increase whenever tracking error e_k along with angular speed ω_k and control input u_k values are sufficiently high, indicating that although ω_k and u_k are high, the large value in e_k is instead due to substantial parametric uncertainty $\boldsymbol{\delta}_k$.

Finally, in a similar fashion to the adaptation in (12), the adaptation law for dynamical model parameters is given by

$$\widehat{\boldsymbol{p}}_k = L[\boldsymbol{d}_k] \tag{14}$$

where

$$\boldsymbol{d}_k = \begin{bmatrix} d_k^0 & d_k^1 \end{bmatrix}^T = \widehat{\boldsymbol{p}}_{k-1} - \frac{\mu_k e_k}{\psi_k} \Gamma \boldsymbol{\xi}_{k-1} \tag{15}$$

and

$$L[\boldsymbol{d}_k] = \begin{cases} \begin{bmatrix} d_k^0 & d_k^1 \end{bmatrix}^T, & \text{if } d_k^1 \geq b_{\min} \\ \begin{bmatrix} d_k^0 & b_{\min} \end{bmatrix}^T, & \text{if } d_k^1 < b_{\min}\ . \end{cases}$$

Introduction of the saturation function $L[\cdot]$ in (14) ensures that $\widehat{\beta}_k$ is lower bounded by $b_{\min}$ and, thus, is nonsingular; T denotes the transpose. Hence, the control algorithm (6) containing $\widehat{\beta}_k^{-1}$ term is bounded.

Based on the above definitions, the following theorem states a convergence bound on the closed-loop error dynamics in (7).

Theorem 1: Under the adaptation law (14) and (15), the closed-loop error dynamics (7) converges to a bound $(\lambda\overline{\eta}c_1/1 - \lambda\overline{\eta}c_2)$ for some nonnegative constants c_1 and c_2 and, $\widehat{\eta}_k \leq \overline{\eta}$ (where k is a nonnegative integer) given that $0 < \lambda < (1/\overline{\eta}c_2)$.

Proof. See the Appendix. ■

III. Experimental Results

To illustrate the efficiency of the proposed adaptive control (6), the control algorithm is tested in experiments and the results obtained are discussed in this section. First, we establish the robotic fish platform on which the proposed control scheme is implemented. Next, the adaptation parameters Γ, γ, and λ are tuned using experimental data to minimize the magnitude of tracking error. Finally, the optimally tuned control scheme is verified to produce desirable reference tracking performance even when the robotic fish payload and drag coefficients are changed.

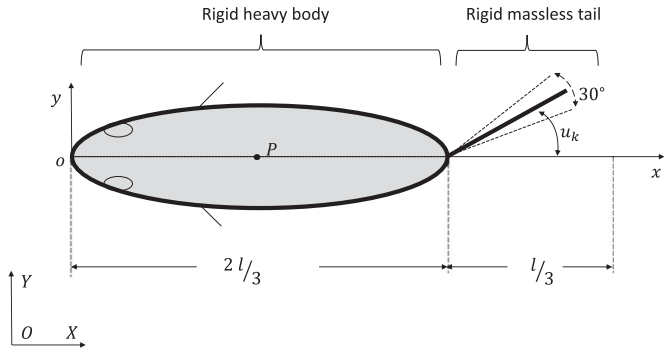

Fig. 2. Free body diagram of a two-link carangiform robotic fish (top view).

A. Robotic Fish Platform

One of the most common styles of biological fish swimming is Carangiform in which the motion thrust is mainly generated by the undulation of the latter one-third part of the fish's body [26], [42]. Mimicking the body style into a robotic fish, a two-link robot structure is created as shown in Fig. 2 representing the top view. Here, x–o–y is marked as the local coordinate axis with origin o as the robot's frontal tip and x-axis passing through the fish's body. The rigid tail of negligible mass is connected to the heavy body via an actuator, which oscillates the tail in the y-direction. The tail of the robot oscillates sinusoidally with a total amplitude of 30° to produce required thrust for forward motion. To control the angular motion, the tail is oscillated at a bias angle u_k from the body axis o–x [18], [38]. The orientation ϕ_k of the fish is defined as the angle made by the o–x axis with reference to the O–X axis.

Based on our exploration, not many literature works examine the angular motion control of a robotic fish. Furthermore, linear motion control of a one-joint robotic fish can be highly complex [30], [31]; and the level of complexity is expected to increase for multijoint robotic fishes. Hence, in this paper, we aim to keep the level of complexity minimal by testing the proposed adaptive control on a one-joint robotic fish.

Although being one-third of the total robot length, the tail is considered massless for simplicity since it weighs just about 29 g as compared to the total robot mass at 490 g (i.e., less than 6% of the robot mass), because the tail is very thin in relation to the robot body and because the robot body carries other heavier items such as the battery, electronic hardware, and balancing weights. This design is inspired from biological fishes where the body is relatively much heavier because it consists of all the essential organs, muscles and dense bones, whereas the tails are very thin and lightweight.

This mechanical structure is realized as a physical model, and its side view is shown in Fig. 3. The total length of the robotic fish l is 0.36 m of which the tail length is 0.12 m. The tail is connected with the rest of the body via a servomotor that provides necessary actuation. Due to mechanical constraints of the motor, the input signal u_k is bounded in the range $[-0.4363, 0.4363]$ rad (i.e., $[-25°, 25°]$). The tail oscillation frequency is kept at 1 Hz, equal to the sampling frequency of the control system. The body is constructed with a light foam alike material to provide sufficient

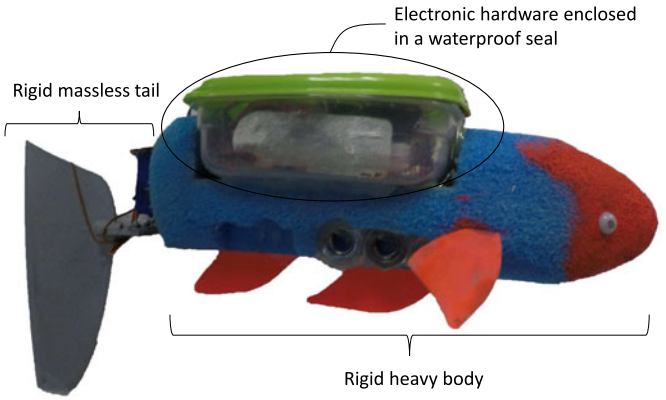

Fig. 3. Physical prototype (side view).

buoyancy and weights are placed at the bottom of the body for stationery stability of the robot in water. A small plastic box is placed on the fish to seal the necessary on board hardware including a battery, microcontroller, voltage regulators, and a wireless communication module.

An overhead camera provides the orientation of the fish w.r.t. the global axis. Using sensor feedback information, a base station, which computes the next control signal and transmits it wirelessly to the on-board microcontroller, then controls the tail oscillation. The experimental trials are conducted in a water pool sized 3×1.8 m^2 and are limited to a time period of 60 s to complete the trials in the available space.

For authentic comparison among the numerous experimental trials conducted, the initial conditions and final reference track are kept constant. Specifically, the initial orientation of the robotic fish is maintained about 0 rad and the initial model parameters are set as $\{\widehat{\alpha}_0, \widehat{\beta}_0\} = \{0.5, 0.5\}$, while the reference orientation is set at 1.5 rad. Although the proposed control can handle the time-varying reference track, the reference orientation is kept constant so that the experiments can be easily conducted in the limited water pool space.

B. Adaptation Parametric Tuning

To maximize the potential of proposed adaptive control technique, it is necessary to optimally tune the adaptation parameters $\{\Gamma, \gamma, \lambda\}$ so as to minimize a cost index value. The cost index is chosen as a summation of tracking error magnitudes, i.e.,

$$\text{cost index} = \sum_k |e_k|$$

because lowering this index value indicates fast convergence of tracking error as well as minimal steady-state error.

In Section II-C, three tunable adaptation parameters, i.e., $\{\Gamma, \gamma, \lambda\}$ are introduced. It is experimentally realized that the adaptation parameters are mutually exclusive cost function variables for the robotic fish motion system; hence, the three parameters are tuned individually. Furthermore, by observing outcomes of a few additional experimental trials, the minimum bound on $\widehat{\beta}_k$, i.e., $b_{\min}$ is determined to be 0.1.

Case 1 (Γ Tuning): Three experimental trials are conducted with Γ being varied as catalogued in Table I, while setting $\gamma = 0.5, \lambda = 0.1$. Note that Γ is chosen as a 2×2 diagonal matrix with equal diagonal elements for simplicity. The reference tracking responses for the three trials are plotted in Fig. 4 and the respective details are tabulated in Table I. It can be easily noticed from Fig. 4 that the control performance is relatively much superior for $\Gamma = 0.9I_2$.

TABLE I
Γ TUNING RESULTS

Γ	Cost index (rad)	Rise time (s)	Steady-state error (rad)
$0.8I_2$	25.15	31.84	0.12
$0.9I_2$	15.12	19.39	0.10
$0.99I_2$	20.16	24.51	0.11

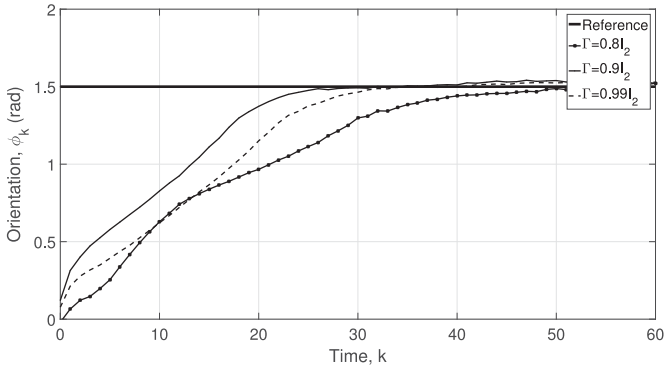

Fig. 4. Experimental results for Γ variation (with $\gamma = 0.5, \lambda = 0.1$).

TABLE II
γ TUNING RESULTS

γ	Cost index (rad)	Rise time (s)	Steady-state error (rad)
0.05	17.58	20.53	0.12
0.1	14.04	15.99	0.12
0.5	15.12	19.39	0.10

From Table I, it is observed that when Γ increases from $0.8I_2$ to $0.9I_2$, the $\sum_k |e_k|$ value significantly decreases from 25.15 to 15.12 rad just as expected because a higher value of Γ leads to rapid adaptation of model parameters in (14) and (15) and, hence, better control performance. In contrast, further increasing Γ to $0.99I_2$ increases the cost index value to 20.16 rad because a very high Γ value can lead to overshoot in the model parameter estimates. Notice that for $\Gamma = 0.9I_2$, even the rise time is relatively very low (see Table I), although steady-state error nearly remains constant. Therefore, based on the above observations, Γ is set as $0.9I_2$ for faster control response.

Case 2 (γ Tuning): By setting $\Gamma = 0.9I_2$ (from above) and $\lambda = 0.1$, another three sets of experimental trials are conducted with γ being $\{0.05, 0.1, 0.5\}$. Reference tracking responses for the three trials are plotted in Fig. 5 and the further required details are catalogued in Table II. Similar to the previous Γ tuning case, from Table I it can again be noticed that increasing the γ from 0.05 to 0.1 decreases the cost index due to faster adaptation of uncertainty bound in (12). However, further increasing γ to

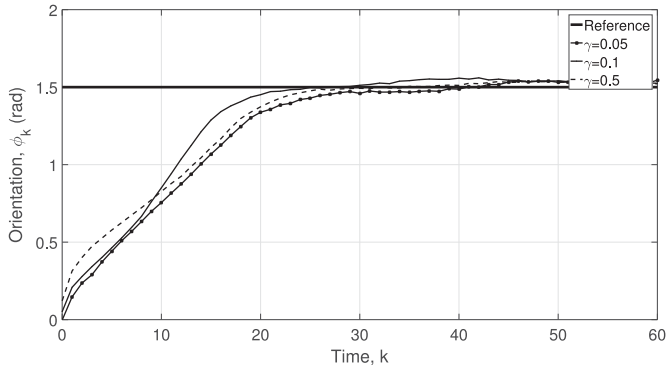

Fig. 5. Experimental results for γ variation (with $\Gamma = 0.9I_2, \lambda = 0.1$).

TABLE III
λ TUNING RESULTS

λ	Cost index (rad)	Rise time (s)	Steady-state error (rad)
0.1	14.04	15.99	0.12
0.01	13.56	14.42	0.11
0.001	15.48	20.64	0.09

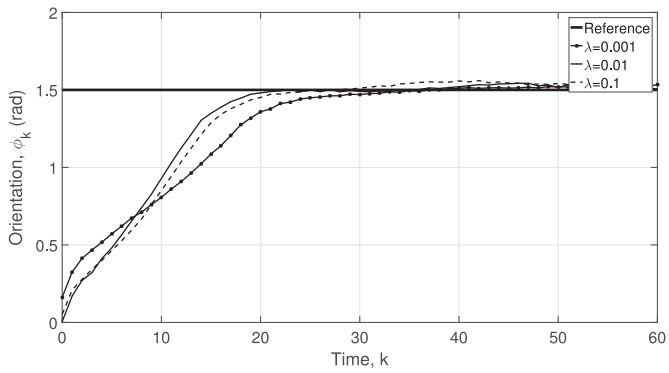

Fig. 6. Experimental results for λ variation (with $\Gamma = 0.9I_2, \gamma = 0.1$).

0.5 slightly increases the cost index likely due to overshoot in parameter estimation. It is also observed that rise time is lowest for $\gamma = 0.1$ (see Table II), although steady-state error remains nearly constant for the three trials. Hence, we set $\gamma = 0.1$ for attaining best control performance.

Case 3 (λ Tuning): Finally, controller performance is analyzed for λ values being $\{10^{-3}, 10^{-2}, 10^{-1}\}$ and is recorded in Table III. Meanwhile, from the previous two cases, we have $\Gamma = 0.9I_2$ and $\gamma = 0.1$. Reference tracking response for the three new experimental trials are plotted in Fig. 6. As discussed earlier, from (9) and (10) it is learned that lowering the λ value should reduce tracking error. Hence, when λ is changed from 0.1 to 0.01, the cost index and rise time values decrease considerably (see Table III). In contradiction, lowering the λ value substantially also reduces adaptation rate in (12), which, in turn, lowers control performance. Therefore, further lowering λ to 0.001 essentially increases cost index and rise time, although slightly reducing the steady-state error (see Table III). On the basis of above analysis, we set $\lambda = 0.01$ for faster adaptation with minimal steady-state error.

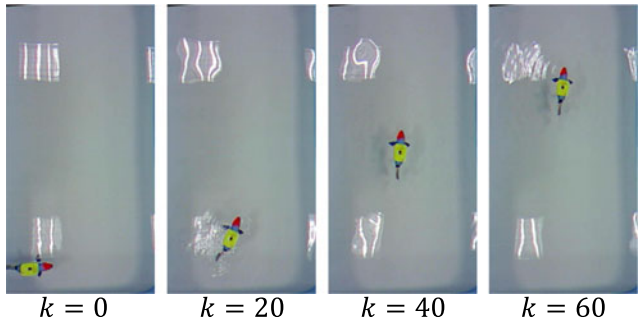

Fig. 7. Robotic fish motion during one of the experimental trials at particular time steps k (top view).

TABLE IV
EXPERIMENTAL OUTCOME UNDER DIFFERENT SCENARIOS

Scenario	Cost index (rad)	Rise time (s)	Steady-state error (rad)
1. No load, no extra drag	13.56	14.42	0.11
2. Load added	15.83	21.42	0.09
3. Drag increased	21.22	23.65	0.17

Therefore under ideal conditions, good control performance is obtained as 13.56 rad cost index, 14.42 s of rise time and 0.11 rad of steady-state error, using $\Gamma = 0.9I_2$, $\gamma = 0.1$, and $\lambda = 0.01$. For this experimental trial, the robotic fish motion for specific periodic time steps is shown in Fig. 7.

Note that from theoretical perspective, all the adaptive law parameters are only required to be positive (or positive definite) and no further conditions are imposed to ensure the stability. However, in the field of control engineering, it is a common practice to fine-tune the parameters of a controller (no matter for a classical controller such as PID or advanced ones such as an adaptive control). Often, by applying fairly minor or moderate efforts in controller detuning, the control system performance can be improved significantly. This can be regarded as the general rule for selecting the tuning parameters. Hence, in our experimental setup, a few trials are conducted just to study a rough range of parametric values and their effect on the controller performance. However, precise tuning of the parameters is not essential for implementation of the proposed adaptive control law.

C. Robustness Against Variations in Environmental Factors

For employment of robotic fishes as potential next generation of AUVs, it is essential that the control algorithms designed must be robust against leading environmental factors. Hence, in this section, the performance of the proposed adaptive control algorithm is experimentally tested in presence of varying environmental factors. Essentially, the control performance is tested under two scenarios, i.e., variations in payload and drag force on the robotic fish.

Table IV compares the controller performance for an additional load of 0.12 g on originally 0.49 g of robotic fish and, added drag force by inserting a thin slit on the robot body perpendicular to its body axis, $o - x$ (see Fig. 2 for notation).

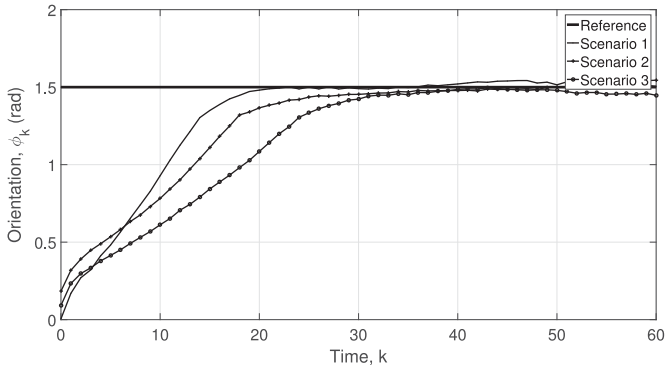

Fig. 8. Orientation profile for different scenarios.

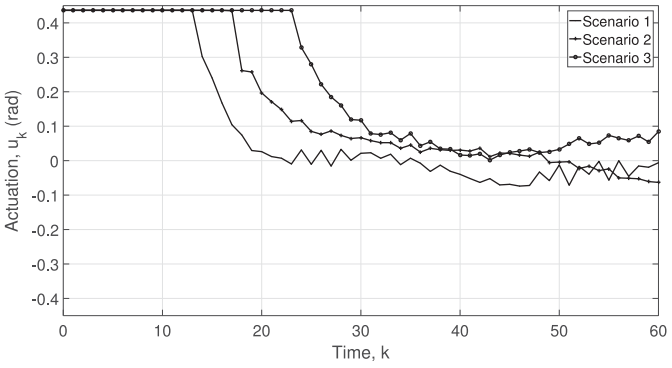

Fig. 9. Actuation profile for different scenarios.

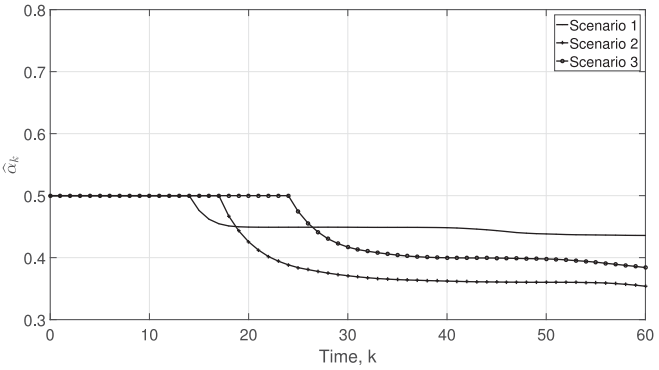

Fig. 10. Model parameter estimate $\widehat{\alpha}_k$ profile for different scenarios.

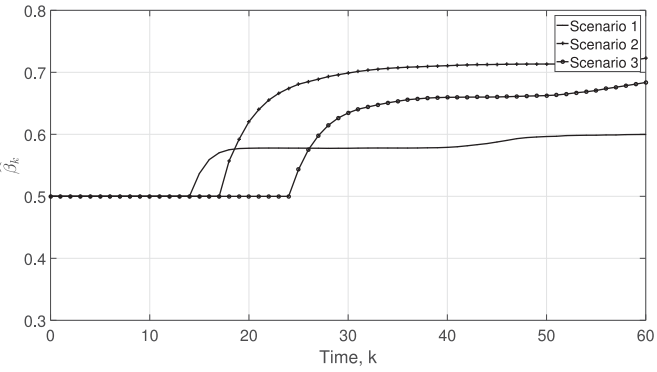

Fig. 11. Model parameter estimate $\widehat{\beta}_k$ profile for different scenarios.

Note that it is very challenging to numerically calculate the amount of drag force increase on the robot, and thus, the drag coefficient a^0 is estimated indirectly via the model parameter a_k in the dynamical model (4). Furthermore, the table also compares with the best performance with no load and extra drag scenario obtained in Section III-B.

First, let us compare results from scenarios 1 and 2. Compared to Scenario 1, load mass is added to the robotic fish in Scenario 2 because of which the inertia of the robotic fish increases and, thus, for the same amount of actuation, the system response is slower. Therefore, it takes more time in Scenario 2 to reach the reference value, and so, the cost index and rise time increase to 15.83 rad and 21.42 s, respectively, in Scenario 2. This effect can also be graphically observed in Fig. 8, which compares the experimental outcome of orientation of the robotic fish under the different scenarios. Note that due to the increased inertia of the robot in Scenario 2, the effect of other external factors on the robotic fish, such as water waves, is minimized. As a result, the steady-state error has lowered in Scenario 2.

Since the robotic fish requires slightly longer duration to reach the reference point, the control input signal also stays high and saturated for longer duration in Scenario 2 as compared with Scenario 1, which can be observed in Fig. 9. After the orientation of the robotic fish reaches close to the reference value, in either scenario, the actuation signal lowers its value quickly and updates within a small bound of $[-0.1, 0.1]$ rad while minimizing the steady-state error.

Next, let us examine results from Scenario 3 in which drag force is increased on the robotic fish body. Observing Figs. 8 and 9, it is evident that the control performance in Scenario 3 is slightly slower than in Scenario 1 or 2. Even though the system response is slower to the actuation because of which it takes slightly longer duration to reach the steady-state value (and hence, the higher cost index value), the overall steady-state error is still acceptably low. Furthermore, from scenarios 2 to 3, the increase in rise time is merely around 2 s (see Table IV).

The above analysis confirms the robustness of the proposed adaptive control to steer the direction of the robotic fish against varying environmental conditions. One of the main factors of providing the robustness by the adaptive control technique is that the model parameter estimates $\{\widehat{\alpha}_k, \widehat{\beta}_k\}$ and uncertainty estimate $\{\widehat{\eta}_k\}$ are rapidly tuned as displayed in Figs. 10–12. Figs. 10 and 11 show that the model parameter estimates settle at slightly different values for the three scenarios considered here, due to the different environmental conditions. In addition, it is observed that the uncertainty in model parameter estimation is very low as observed from Fig. 12.

Note in the figures that the adaptation is halted temporarily, i.e., the estimated values are kept constant for the earlier 15–25 s of the experimental trials until respective control signal becomes unsaturated (see Fig. 9). This practical approach is helpful in preventing overshoot in the model parameter estimates because when the control signal is saturated, unnecessary adaptation in parameters cannot further physically increase the control signal to reduce the tracking error rapidly.

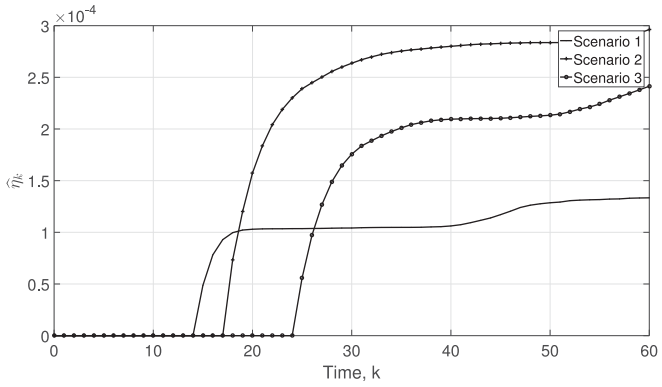

Fig. 12. Uncertainty estimate $\widehat{\eta}_k$ profile for different scenarios.

IV. Conclusion

In this paper, an adaptive control technique is proposed for orientation control of a robotic fish. First, the dynamical model is derived in LIPs form by linearization of a nonlinear model. Second, inverse dynamics are implemented for attaining the respective controller form. Next, the model parameters are adapted using a robust adaptation technique based on the minimization of parametric estimation uncertainties. With rigorous convergence analysis, it is shown that the error in orientation tracking is also bounded within a prescribed bound. The adaptation parameters are experimentally tuned and the robustness of the proposed adaptive control is experimentally verified in different scenarios. In our future works, the adaptive control approach will be extended toward the 3-D motion control of the robotic fish.

Appendix
Proof of Theorem 1

Consider a nonnegative function

$$V_k \triangleq \widetilde{\boldsymbol{p}}_k^T \Gamma^{-1} \widetilde{\boldsymbol{p}}_k + \frac{1}{\gamma}\widetilde{\eta}_k^2$$

and its variation at every time instant given by

$$\begin{aligned}\Delta V_k &= V_k - V_{k-1} \\ &= \widetilde{\boldsymbol{p}}_k^T \Gamma^{-1} \widetilde{\boldsymbol{p}}_k - \widetilde{\boldsymbol{p}}_{k-1}^T \Gamma^{-1} \widetilde{\boldsymbol{p}}_{k-1} + \frac{1}{\gamma}\left(\widetilde{\eta}_k^2 - \widetilde{\eta}_{k-1}^2\right). \quad (16)\end{aligned}$$

Here, the uncertainty estimation error is defined as $\widetilde{\eta}_k \triangleq \eta_k - \widehat{\eta}_k$. Furthermore, importing the definition of $\widehat{\eta}_k$ from (12), we have

$$\widetilde{\eta}_k = \widetilde{\eta}_{k-1} - \frac{\mu_k \sigma_{k-1} \gamma \lambda \|\boldsymbol{\xi}_{k-1}\| |e_k|}{\psi_k}. \quad (17)$$

In addition, from (5) and (14), we note that $\widetilde{\boldsymbol{p}}_k = \boldsymbol{p}_* - L[\boldsymbol{d}_k]$, where $\boldsymbol{d}_k$ is previously defined in (15). Furthermore, since $b_k \geq b_{\min}$, the following holds true:

$$\begin{aligned}|b_k - b_{\min}| &\leq |b_k - d_k^1| \\ \|\boldsymbol{p}_* - L[\boldsymbol{d}_k]\| &\leq \|\boldsymbol{p}_* - \boldsymbol{d}_k\|\end{aligned}$$

and hence for the positive definite matrix Γ^{-1}

$$\begin{aligned}\widetilde{\boldsymbol{p}}_k^T \Gamma^{-1} \widetilde{\boldsymbol{p}}_k &= (\boldsymbol{p}_* - L[\boldsymbol{d}_k])^T \Gamma^{-1} (\boldsymbol{p}_* - L[\boldsymbol{d}_k]) \\ &\leq (\boldsymbol{p}_* - \boldsymbol{d}_k)^T \Gamma^{-1} (\boldsymbol{p}_* - \boldsymbol{d}_k). \quad (18)\end{aligned}$$

Therefore, using relations in (17) and (18), the equation in (16) can be updated to

$$\begin{aligned}\Delta V_k &\leq (\boldsymbol{p}_* - \boldsymbol{d}_k)^T \Gamma^{-1} (\boldsymbol{p}_* - \boldsymbol{d}_k) - \widetilde{\boldsymbol{p}}_{k-1}^T \Gamma^{-1} \widetilde{\boldsymbol{p}}_{k-1} \\ &\quad + \frac{1}{\gamma}\left(\left(\widetilde{\eta}_{k-1} - \frac{\mu_k \gamma \lambda \|\boldsymbol{\xi}_{k-1}\| |e_k|}{\psi_k}\right)^2 - \widetilde{\eta}_{k-1}^2\right) \\ &\leq \left(\widetilde{\boldsymbol{p}}_{k-1} + \frac{\mu_k e_k}{\psi_k}\Gamma \boldsymbol{\xi}_{k-1}\right)^T \Gamma^{-1} \times \left(\widetilde{\boldsymbol{p}}_{k-1} + \frac{\mu_k e_k}{\psi_k}\Gamma \boldsymbol{\xi}_{k-1}\right) \\ &\quad + \frac{1}{\gamma}\left(\widetilde{\eta}_{k-1} - \frac{\mu_k \gamma \lambda \|\boldsymbol{\xi}_{k-1}\| |e_k|}{\psi_k}\right)^2 \\ &\quad - \widetilde{\boldsymbol{p}}_{k-1}^T \Gamma^{-1} \widetilde{\boldsymbol{p}}_{k-1} - \frac{1}{\gamma}\widetilde{\eta}_{k-1}^2 \\ &\leq \frac{2\mu_k e_k}{\psi_k}\widetilde{\boldsymbol{p}}_{k-1}^T \boldsymbol{\xi}_{k-1} - \frac{2\mu_k \lambda \|\boldsymbol{\xi}_{k-1}\| |e_k| \widetilde{\eta}_{k-1}}{\psi_k} \\ &\quad + \frac{\mu_k^2 e_k^2}{\psi_k^2}\left(\boldsymbol{\xi}_{k-1}^T \Gamma \boldsymbol{\xi}_{k-1} + \gamma \lambda^2 \|\boldsymbol{\xi}_{k-1}\|^2\right). \quad (19)\end{aligned}$$

From the closed-loop error dynamics (7), we have

$$e_k + \widetilde{\boldsymbol{p}}_{k-1}^T \boldsymbol{\xi}_{k-1} = -\boldsymbol{\delta}_{k-1}^T \boldsymbol{\xi}_{k-1}$$

and since (10) states $\|\boldsymbol{\delta}_{k-1}\| \leq \lambda \eta$, i.e., $\|\boldsymbol{\delta}_{k-1}^T \boldsymbol{\xi}_{k-1} e_k\| \leq \lambda \eta \|\boldsymbol{\xi}_{k-1}\| |e_k|$, further we have

$$e_k^2 + e_k \widetilde{\boldsymbol{p}}_{k-1}^T \boldsymbol{\xi}_{k-1} \leq \lambda \eta \|\boldsymbol{\xi}_{k-1}\| |e_k|. \quad (20)$$

Hence, utilizing relations in (13) and (20), (19) updates to

$$\Delta V_k \leq -\frac{2\mu_k}{\psi_k}\left(e_k^2 - \lambda \widehat{\eta}_{k-1} \|\boldsymbol{\xi}_{k-1}\| |e_k|\right) + \frac{\mu_k^2 e_k^2}{\psi_k} \cdot \frac{\psi_k - 1}{\psi_k}. \quad (21)$$

From the definition of μ_k (11), when $|e_k| \geq \lambda \widehat{\eta}_{k-1} \|\boldsymbol{\xi}_{k-1}\|$, we have

$$\mu_k e_k^2 = e_k^2 - \lambda \widehat{\eta}_{k-1} \|\boldsymbol{\xi}_{k-1}\| |e_k|$$

Furthermore, notice that $(\psi_k - 1)/\psi_k < 1$ [as per ψ_k definition (13)], and thus, (21) reduces to

$$\Delta V_k < -\frac{\mu_k^2 e_k^2}{\psi_k}$$

which indicates that $\widehat{\boldsymbol{p}}_k$ and $\widehat{\eta}_k$ are bounded because V_k is nonincreasing. Furthermore,

$$V_k = V_0 + \sum_{i=1}^{k} \Delta V_i$$

$$V_k < V_0 - \sum_{i=1}^{k} \frac{2\mu_k^2 e_k^2}{\psi_k}$$

and because V_k is nonnegative and V_0 is bounded

$$\lim_{k\to\infty} \frac{2\mu_k^2 e_k^2}{\psi_k} = 0. \tag{22}$$

Now, notice that from (8), we have

$$\|\boldsymbol{\xi}_k\| \leq |\phi_k - \phi_{k-1}| + \left|\widehat{\beta}_k^{-1}\left(\phi_{k+1}^r - (1+\widehat{\alpha}_k)\phi_k + \widehat{\alpha}_k\phi_{k-1}\right)\right|.$$

Adding and subtracting reference signal from the above, it follows:

$$\begin{aligned}\|\boldsymbol{\xi}_k\| &\leq |e_k - e_{k-1}| + |\phi_k^r - \phi_{k-1}^r| \\ &\quad + \left|\widehat{\beta}_k^{-1}\left(-(1+\widehat{\alpha}_k)e_k + \widehat{\alpha}_k e_{k-1}\right)\right| \\ &\quad + \left|\widehat{\beta}_k^{-1}\left(\phi_{k+1}^r - (1+\widehat{\alpha}_k)\phi_k^r + \widehat{\alpha}_k\phi_{k-1}^r\right)\right| \\ &\leq c_1 + c_2|e_k| + c_3|e_{k-1}| \end{aligned} \tag{23}$$

for some bounded nonnegative constants c_1, c_2, and c_3. The boundedness of these constants requires boundedness of $\widehat{\alpha}_k$ and $\widehat{\beta}_k$, which holds true due to boundedness of V_k from above. Adding and subtracting reference signal from the dynamical model in (4), it is easy to derive

$$\begin{aligned}e_{k+1} &= (1+a_k)e_k - a_k e_{k-1} + b_k u_k \\ &\quad + \left(\phi_{k+1}^r - (1+a_k)\phi_k^r + a_k\phi_{k-1}^r\right).\end{aligned}$$

Therefore, (23) can be updated to

$$\|\boldsymbol{\xi}_k\| \leq c_4 + c_5|e_{k+1}| \tag{24}$$

for some bounded nonnegative constants c_4 and c_5. As a consequence, from the definition in (13), ψ_k is in the order of e_k^2.

Hence, from (13) and (24), it is obtained that ψ_k is in the order of e_k^2. Therefore, (22) satisfies the key technical lemma in [43], which guarantees that $\mu_k e_k \to 0$ as $k \to \infty$ [39]. Additionally, it states that there must exist ρ such that $\max_{j\in[0,k]}(\mu_j e_j) \leq \rho$. Then, by the definition of μ_k (11), the following must hold true:

$$\begin{aligned}\max_{j\in[0,k]}|e_j| &\leq \rho + \lambda\overline{\eta}\max_{j\in[0,k]}(c_4 + c_5|e_j|) \\ &\leq \frac{\rho + \lambda\overline{\eta}c_4}{1-\lambda\overline{\eta}c_5}\end{aligned}$$

where $\widehat{\eta}_k \leq \overline{\eta}\,\forall k \in \{0,1,2,\dots\}$. Hence, the reference tracking error is bounded when

$$0 < \lambda < \frac{1}{\overline{\eta}c_5}.$$

Finally, as $\mu_k e_k \to 0$ for $k \to \infty$

$$\lim_{k\to\infty}|e_k| \leq \frac{\lambda\overline{\eta}c_4}{1-\lambda\overline{\eta}c_5}.$$

REFERENCES

[1] M. S. Triantafyllou and G. S. Triantafyllou, "An efficient swimming machine," *Sci. Amer.*, vol. 272, no. 3, pp. 64–71, Mar. 1995.

[2] M. Sfakiotakis, D. M. Lane, and J. B. C. Davies, "Review of fish swimming modes for aquatic locomotion," *IEEE J. Ocean. Eng.*, vol. 24, no. 2, pp. 237–252, Apr. 1999.

[3] J. Yu, M. Tan, S. Wang, and E. Chen, "Development of a biomimetic robotic fish and its control algorithm," *IEEE Trans. Syst., Man, Cybern. B, Cybern.*, vol. 34, no. 4, pp. 1798–1810, Aug. 2004.

[4] M. A. MacIver, E. Fontaine, and J. W. Burdick, "Designing future underwater vehicles: Principles and mechanisms of the weakly electric fish," *IEEE J. Ocean. Eng.*, vol. 29, no. 3, pp. 651–659, Jul. 2004.

[5] A. Crespi, D. Lachat, A. Pasquier, and A. J. Ijspeert, "Controlling swimming and crawling in a fish robot using a central pattern generator," *Auton. Robots*, vol. 25, no. 1/2, pp. 3–13, Aug. 2008.

[6] S. Shatara and X. Tan, "An efficient, time-of-flight-based underwater acoustic ranging system for small robotic fish," *IEEE J. Ocean. Eng.*, vol. 35, no. 4, pp. 837–846, Oct. 2010.

[7] I. Vasilescu *et al.*, "Amour V: A hovering energy efficient underwater robot capable of dynamic payloads," *Int. J. Robot. Res.*, vol. 29, no. 5, pp. 547–570, Apr. 2010.

[8] Y. Xu and K. Mohseni, "A pressure sensory system inspired by the fish lateral line: Hydrodynamic force estimation and wall detection," *IEEE J. Ocean. Eng.*, vol. 42, no. 3, pp. 532–543, Jul. 2017.

[9] A. D. Marchese, C. D. Onal, and D. Rus, "Autonomous soft robotic fish capable of escape maneuvers using fluidic elastomer actuators," *Soft Robot.*, vol. 1, no. 1, pp. 75–87, Feb. 2014.

[10] J. J. Hubbard, M. Fleming, V. Palmre, D. Pugal, K. J. Kim, and K. K. Leang, "Monolithic IPMC fins for propulsion and maneuvering in bioinspired underwater robotics," *IEEE J. Ocean. Eng.*, vol. 39, no. 3, pp. 540–551, Jul. 2014.

[11] D. Shin, S. Y. Na, J. Y. Kim, and S.-J. Baek, "Fuzzy neural networks for obstacle pattern recognition and collision avoidance of fish robots," *Soft Comput.*, vol. 12, no. 7, pp. 715–720, 2008. [Online]. Available: http://dx.doi.org/10.1007/s00500-007-0245-0

[12] Y. Hu, W. Zhao, and L. Wang, "Vision-based target tracking and collision avoidance for two autonomous robotic fish," *IEEE Trans. Ind. Electron.*, vol. 56, no. 5, pp. 1401–1410, May 2009.

[13] Y. Jia and L. Wang, "Leader-follower flocking of multiple robotic fish," *IEEE/ASME Trans. Mechatron.*, vol. 20, no. 3, pp. 1372–1383, Jun. 2015.

[14] J. Yu, C. Wang, and G. Xie, "Coordination of multiple robotic fish with applications to underwater robot competition," *IEEE Trans. Ind. Electron.*, vol. 63, no. 2, pp. 1280–1288, Feb. 2016.

[15] H. E. Daou, T. Salumae, L. D. Chambers, W. M. Megill, and M. Kruusmaa, "Modelling of a biologically inspired robotic fish driven by compliant parts," *Bioinspiration Biomimetics*, vol. 9, no. 1, Jan. 2014, Art. no. 016010.

[16] C. Hemelrijk, D. Reid, H. Hildenbrandt, and J. Padding, "The increased efficiency of fish swimming in a school," *Fish Fisheries*, vol. 16, no. 3, pp. 511–521, Sep. 2014.

[17] J. Kim, H. Joe, S. C. Yu, J. S. Lee, and M. Kim, "Time-delay controller design for position control of autonomous underwater vehicle under disturbances," *IEEE Trans. Ind. Electron.*, vol. 63, no. 2, pp. 1052–1061, Feb. 2016.

[18] P. Suebsaiprom and C.-L. Lin, "Maneuverability modeling and trajectory tracking for fish robot," *Control Eng. Practice*, vol. 45, pp. 22–36, Dec. 2015.

[19] Y. Hu, J. Liang, and T. Wang, "Parameter synthesis of coupled nonlinear oscillators for CPG-based robotic locomotion," *IEEE Trans. Ind. Electron.*, vol. 61, no. 11, pp. 6183–6191, Nov. 2014.

[20] X. Niu, J. Xu, Q. Ren, and Q. Wang, "Locomotion generation and motion library design for an anguilliform robotic fish," *J. Bionic Eng.*, vol. 10, no. 3, pp. 251–264, Jul. 2013.

[21] L. Wen, T. Wang, G. Wu, and J. Liang, "Quantitative thrust efficiency of a self-propulsive robotic fish: Experimental method and hydrodynamic investigation," *IEEE/ASME Trans. Mechatron.*, vol. 18, no. 3, pp. 1027–1038, Jun. 2013.

[22] T. Hu, K. H. Low, L. Shen, and X. Xu, "Effective phase tracking for bioinspired undulations of robotic fish models: A learning control approach," *IEEE/ASME Trans. Mechatron.*, vol. 19, no. 1, pp. 191–200, Feb. 2014.

[23] M. Porez, F. Boyer, and A. J. Ijspeert, "Improved lighthill fish swimming model for bio-inspired robots: Modeling, computational aspects and experimental comparisons," *Int. J. Robot. Res.*, vol. 33, no. 10, pp. 1322–1341, Sep. 2014.

[24] J. Wang and X. Tan, "A dynamic model for tail-actuated robotic fish with drag coefficient adaptation," *Mechatronics*, vol. 23, no. 6, pp. 659–668, Sep. 2013.

[25] Q. Ren, J. Xu, and X. Li, "A data-driven motion control approach for a robotic fish," *J. Bionic Eng.*, vol. 12, no. 3, pp. 382–394, Jul. 2015.

[26] J. Yu, M. Wang, Z. Su, M. Tan, and J. Zhang, "Dynamic modeling of a CPG-governed multijoint robotic fish," *Adv. Robot.*, vol. 27, no. 4, pp. 275–285, Mar. 2013.

[27] H. Li, P. Xie, and W. Yan, "Receding horizon formation tracking control of constrained underactuated autonomous underwater vehicles," *IEEE Trans. Ind. Electron.*, vol. 64, no. 6, pp. 5004–5013, Jun. 2017.
[28] J. Yu, J. Yuan, Z. Wu, and M. Tan, "Data-driven dynamic modeling for a swimming robotic fish," *IEEE Trans. Ind. Electron.*, vol. 63, no. 9, pp. 5632–5640, Sep. 2016.
[29] L. Wen, T. Wang, G. Wu, J. Liang, and C. Wang, "Novel method for the modeling and control investigation of efficient swimming for robotic fish," *IEEE Trans. Ind. Electron.*, vol. 59, no. 8, pp. 3176–3188, Aug. 2012.
[30] X. Li, Q. Ren, and J. X. Xu, "Precise speed tracking control of a robotic fish via iterative learning control," *IEEE Trans. Ind. Electron.*, vol. 63, no. 4, pp. 2221–2228, Apr. 2016.
[31] S. Verma, J. X. Xu, Q. Ren, W. B. Tay, and F. Lin, "A comparison of robotic fish speed control based on analytical and empirical models," in *Proc. 42nd Annu. Conf. IEEE Ind. Electron. Soc.*, Oct. 2016, pp. 6055–6060.
[32] P. E. Pounds, D. R. Bersak, and A. M. Dollar, "Stability of small-scale UAV helicopters and quadrotors with added payload mass under PID control," *Auton. Robots*, vol. 33, no. 1/2, pp. 129–142, Aug. 2012.
[33] J.-H. Kim, J.-Y. Kim, and J.-H. Oh, "Adaptive walking pattern generation and balance control of the passenger-carrying biped robot, HUBO FX-1, for variable passenger weights," *Auton. Robots*, vol. 30, no. 4, pp. 427–443, May 2011.
[34] W. L. Chan and T. Kang, "Simultaneous determination of drag coefficient and added mass," *IEEE J. Ocean. Eng.*, vol. 36, no. 3, pp. 422–430, Jul. 2011.
[35] H. Zhao, X. Liu, D. Li, A. Wei, K. Luo, and J. Fan, "Vortex dynamics of a sphere wake in proximity to a wall," *Int. J. Multiphase Flow*, vol. 79, no. 1, pp. 88–106, Feb. 2016.
[36] M. R. Jardin and E. R. Mueller, "Optimized measurements of unmanned-air-vehicle mass moment of inertia with a bifilar pendulum," *J. Aircraft*, vol. 46, no. 3, pp. 763–775, May 2009.
[37] Z. Su, J. Yu, M. Tan, and J. Zhang, "Implementing flexible and fast turning maneuvers of a multijoint robotic fish," *IEEE/ASME Trans. Mechatron.*, vol. 19, no. 1, pp. 329–338, Feb. 2014.
[38] J. Yu, C. Zhang, and L. Liu, "Design and control of a single-motor-actuated robotic fish capable of fast swimming and maneuverability," *IEEE/ASME Trans. Mechatron.*, vol. 21, no. 3, pp. 1711–1719, Jun. 2016.
[39] K. Abidi, "A robust discrete-time adaptive control approach for systems with almost periodic time-varying parameters," *Int. J. Robust Nonlinear Control*, vol. 24, no. 1, pp. 166–178, Jan. 2014.
[40] W. Wang and G. Xie, "Online high-precision probabilistic localization of robotic fish using visual and inertial cues," *IEEE Trans. Ind. Electron.*, vol. 62, no. 2, pp. 1113–1124, Feb. 2015.
[41] J. Yu, F. Sun, D. Xu, and M. Tan, "Embedded vision-guided 3-d tracking control for robotic fish," *IEEE Trans. Ind. Electron.*, vol. 63, no. 1, pp. 355–363, Jan. 2016.
[42] R. W. Blake, *Fish Locomotion*. Cambridge, U.K.: Cambridge Univ. Press, May 1983.
[43] G. C. Goodwin and K. S. Sin, *Adaptive Filtering Prediction and Control*. North Chelmsford, MA, USA: Courier, 2014.

Saurab Verma (S'15) received the B.S. degree in electrical and electronics engineering and the M.S. degree in physics from the Birla Institute of Technology and Science, Pilani, India, in 2014. He is currently working toward the Ph.D. degree in the Department of Electrical and Computer Engineering, National University of Singapore, Singapore.

His research interest lies in the area of motion control, dynamical analysis, intelligence, and navigation of robots.

Dong Shen (M'10) received the B.S. degree in mathematics from Shandong University, Jinan, China, in 2005 and the Ph.D. degree in mathematics from the Academy of Mathematics and System Science, Chinese Academy of Sciences (CAS), Beijing, China, in 2010.

From 2010 to 2012, he was a Postdoctoral Fellow with the Institute of Automation, CAS. From 2016 to 2017, he was a Visiting Scholar at the National University of Singapore, Singapore. Since 2012, he has been an Associate Professor with the College of Information Science and Technology, Beijing University of Chemical Technology, Beijing, China. His current research interests include iterative learning controls, stochastic control, and optimization. He has published more than 60 refereed journal and conference papers. He is the author of *Stochastic Iterative Learning Control* (Science Press, 2016, in Chinese) and the coauthor of *Iterative Learning Control for Multi-Agent Systems Coordination* (New York, NY, USA: Wiley, 2017).

Dr. Shen received the IEEE Control Systems Society (CSS) Beijing Chapter Young Author Prize in 2014 and the Wentsun Wu Artificial Intelligence Science and Technology Progress Award in 2012.

Jian-Xin Xu (F'11) received the B.S. degree from Zhejiang University, China, in 1982 and the M.S. and Ph.D. degrees from the University of Tokyo, Tokyo, Japan, in 1986 and 1989 respectively, all in electrical engineering.

In 1991, he joined the Department of Electrical Engineering, National University of Singapore, Singapore, where he currently serves as a Professor. His research interests lie in the fields of learning theory, intelligent control, nonlinear and robust control, robotics, and precision motion control. He has published more than 170 journal papers and five books in the field of system and control.